Adaptive moving grids in problems of gas dynamics [1)].

© Boris N. Azarenok

Computing Center of Russian Academy of Sciences,
Vavilov str. 40, Moscow, 117967, Russia
E-mail: azarenok@ccas.ru

Abstract. Application of harmonic mapping using a variational approach in order to generate moving adaptive grids in the hyperbolic problems of gas dynamics is considered. Three-point model of adaptation shows if control/(monitor) function is discontinuous, minimizing the discrete analogy of the harmonic functional it is provided possibility to generate an unfolded mesh with strong grid lines condensing in the vicinity of shocks. The algorithm of moving the boundary nodes is suggested consisting in using constrained minimization of the functional when constraints define the boundary of the domain. Computational tests of the unsteady flow in a tunnel containing a step and transonic and supersonic flow over an airfoil demonstrate possibility to control mesh sizes across shocks and contact discontinuities.

Key words. Adaptive grid, variational barrier method, harmonic mapping, constrained optimization

Introduction. In the present study it is considered some theoretical aspects and practical possibilities of using the moving grid technology in hyperbolic problems of gas dynamics with discontinuous solution. The essence of such an approach, referred as r-refinement, is in adjusting distribution of the grid nodes in such a manner so that to catch nuances of interest in the solution with fixed computer cost. Constructive way is that we try to position more grid nodes in the domains of sharp change in the solution being the regions of great gradients, while the mesh structure remains invariable that makes more simple the course of computation. Examples of some r-refinement based methods can be found in [10, 7, 9, 4].

One of the mesh generation techniques is a variational approach when minimizing the Dirichlet (or harmonic) functional of smoothness, first applied in [11], we ensure the grid lines to be as smooth as possible [3]. To

[1)] This work was supported by the Russian Fund of Fundamental Research (project code 99-01-00264)

include adaptivity in this process it has been suggested to write the Dirichlet functional on the surface of the control/(monitor) function, being the solution of the basic problem or somehow connected with it [8]. In [6] approximation the functional is performed in such a way that in case of smooth solution there is an infinite barrier ensuring the mesh to be convex, in other words all grid cells to be convex quadrilaterals. In [1, 2] adaptive-harmonic grid generation has been applied in 2-D unsteady problems of gas dynamics.

1. Problem Formulation. To generate the 2-D adaptive-harmonic mesh we use the formulation of the problem on minimizing the harmonic functional of smoothness written on a surface of some control function $f(x, y)$ [6]

(1)
$$I = \int\int \frac{(x_\xi^2 + x_\eta^2)(1+c_a^2 f_x^2)+(y_\xi^2+y_\eta^2)(1+c_a^2 f_y^2)+2c_a^2 f_x f_y (x_\xi y_\xi + x_\eta y_\eta)}{(x_\xi y_\eta - x_\eta y_\xi)\sqrt{1 + c_a^2 f_x^2 + c_a^2 f_y^2}} d\xi d\eta \, .$$

The task in hand is to find the functions $x(\xi, \eta)$ and $y(\xi, \eta)$ ensuring one-to-one inverse mapping of the parametric square $0<\xi, \eta<1$ to a physical domain Ω by minimizing the functional (1). Here c_a is the coefficient of adaptation, showing that we work with the control function multiplied by some coefficient c_a in order to increase or decrease adaptation.

In 1-D case to generate the inverse harmonic mapping of the graph of f to the unit segment in logic space ξ it is required to minimize the following functional:

(2)
$$I = \int \frac{1}{x_\xi \sqrt{1 + c_a^2 f_x^2}} d\xi .$$

Minimizing (2) we seek the grid points arc-length equidistribution in metric of the curve $c_a f$.

2. Approximation of functional. The functional (1) can be approximated in such a way that its minimum is attained on a grid of convex quadrilaterals [6, 5]

(3)
$$I^h = \sum_{i=1}^{i_{max}} \sum_{k=1}^{4} \frac{1}{4} [F_k]_i \, ,$$

where F_k is the integrand evaluated in the k-th corner of the i-th cell. It has been shown when generating a curvilinear mesh in an arbitrary domain

Ω in plane $x-y$ the discrete functional I^h, approximating (2) on the mesh formed with quadrilateral cells, has an infinite barrier on the boundary of the set of grids with all convex cells. This is caused by the condition of positiveness to the expression $x_\xi y_\xi - x_\eta y_\eta$ in (1), being the Jacobian of the mapping. Should the vertexes of some cell displace so that the cell becomes nearly nonconvex, then one of four triangles, into which the cell is divided by its two diagonals, degenerates, its area tends to zero and, therefore, $I^h \to \infty$. This holds in case of adaptive grid generation as well when the control function $f \in C^1(\Omega)$ since the values f_x, f_y under the square root in (1) are restricted everywhere in Ω. However, if f belongs to the class of discontinuous functions, what we generally have in hyperbolic problems of gas dynamics, in the vicinity of a discontinuity the derivatives f_x, f_y become unbounded. Therefore, the above infinite barrier disappears and this causes some grid cells to fold and modeling to break. In order to prevent grid lines overlap it will be used the procedure of regularization to the discrete functional.

Discretized 1-D functional (2) reads

$$I^h = \sum_{i=1}^{i_{max}} \frac{\triangle \xi}{(x_\xi)_{i+1/2} \sqrt{1 + c_a^2 (f_x)^2_{i+1/2}}} , \tag{4}$$

3. Three-Point Model of Adaptation. Consider 1-D adaptive mesh generation. We solve the Cauchy problem to the nonlinear advection equation with discontinuous initial data, i.e., initial value problem (IVP) when the shock moves from the left to the right

$$\frac{\partial u}{\partial t} + u \frac{\partial u}{\partial x} = 0 , \quad u(x,0) = \{u_l, \text{ if } x < 0; \ u_r, \text{ if } x \geq 0; \ u_l > u_r\} . \tag{5}$$

In plane $x-y$ we introduce the moving grid, see Fig.1a. To update the discrete function value $u^{i+1/2}$ at time t^{n+1} we use the Godunov's scheme on the moving grid. The following theorem holds

Theorem. *Let without adaptation the grid nodes move with speed of shock* $w=0.5(u_r+u_l)$. *Suppose at time* t^n *the shock is smeared over two cells, i.e.,* $u_{i+1/2}=u_l$ *if* $i<i_c$ *and* $u_{i+1/2}=u_r$ *if* $i \geq i_c$, *where* i_c *is a node being the center of the shock smeared and the average mesh node, i.e.,* $i_c=0.5 i_{max}+1$, *where* i_{max} *is an even number of intervals. Then the updated values* $u^{i+1/2}$ *do not change.*

Consequently, when adapting the mesh we need not solve IVP (5) and can merely set the values equal u_l to the left of the i_c-th point and u_r to the right.

We shall construct the adapted mesh minimizing the functional (2) and use u as a control function. For the sake of simplicity we consider the left half of the mesh consisting of three points, i.e., when i_c=3. Such an assumption does not change the structure of the solution. The general case can be easy obtained from this three-point model.

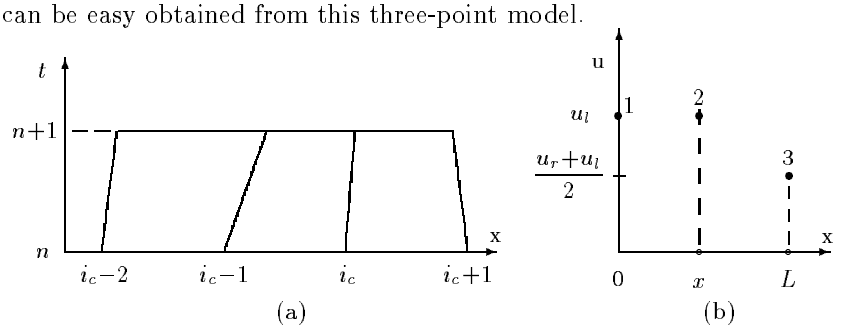

Fig.1. Moving grid (a); i_c is a center of the shock smeared. Three-point model of adaptation (b); in the coordinate system, moving with speed of shock w, x_1=0 and x_3=L are the coordinates of the fixed boundary nodes, x_2=x is a moving node.

We pass into the new coordinate system moving with velocity w so that x_1=0, see Fig.1b. Then when adapting 1 and 3 are the fixed boundary nodes and x_3=L, where L=2h, h is a spacing of the initial uniform mesh, coordinate x_2 is variable, referred further as x. We also have u_1=u_2=u_l , u_3=$(u_l + u_r)/2$.

4. Properties of discrete functional. Consider the properties of the discrete functional in 1-D and 2-D cases within the framework of three-point model of adaptation.

First, consider 1-D case. In assumptions of Section 3 the approximation (4) to the functional on the two-cell grid reads (we set $\triangle\xi = 1$ and use the simple finite-difference approximations to $(x_\xi)_{i+1/2}$ and $(f_x)_{i+1/2}$)

$$I^h = \frac{1}{x} + \frac{1}{(L-x)\sqrt{1 + c_a^2 \triangle u^2/(L-x)^2}}\,, \tag{6}$$

where $\triangle u$=$|u_3 - u_2|/2$=$|u_r - u_l|/2$. To minimize the one-parametric functional I^h we apply the Newton method

$$x^{p+1} = x^p - \tau \frac{\partial I^h}{\partial x} \left[\frac{\partial^2 I^h}{\partial x^2}\right]^{-1}\,, \tag{7}$$

where the iterative parameter $\tau \leq 1$, the first derivative is

$$\frac{\partial I^h}{\partial x} = -\frac{1}{x^2} + \frac{1}{(L-x)^2\left[1 + c_a^2 \triangle u^2/(L-x)^2\right]^{3/2}},$$

and the second derivative is derived of the first one.

In Fig.2 distributions of I^h and $\partial I^h/\partial x$ are presented for several values of c_a at u_l=2, u_r=1 and initial uniform spacing h=0.1. One can see at c_a=0 the functional I^h has the minimum at x=0.1 that corresponds to the points equidistribution or uniform mesh. At c_a>0 the functional I^h loses its convexity in the interval $(0, 0.2)$ since there is a maximum to the left from point 3. Therefore, solution of the variational problem on finding its extremum becomes non-unique. When increasing c_a on one hand the minimum of I^h shifts to the right that corresponds to point 2 moving towards point 3 or grid clustering, see Fig.2b, on the other hand the maximum of I^h shifts to the left from point 3 causing grid rarefaction. In 2-D problems it can cause harsh displacements of the mesh nodes due to jumps of the solution from the minimum to maximum and vice versa during iterations, i.e., grid foldness and instability in the solution of the flow problem. Furthermore, on achieving the critical value $c_a^{crt} \simeq 0.185$ the both extrema merge and further at $c_a > c_a^{crt}$ they disappear, see the curve c_a=0.2 in Fig.2b. Minimization of I^h causes the right cell to collapse, consequently, significant mesh clustering is impossible.

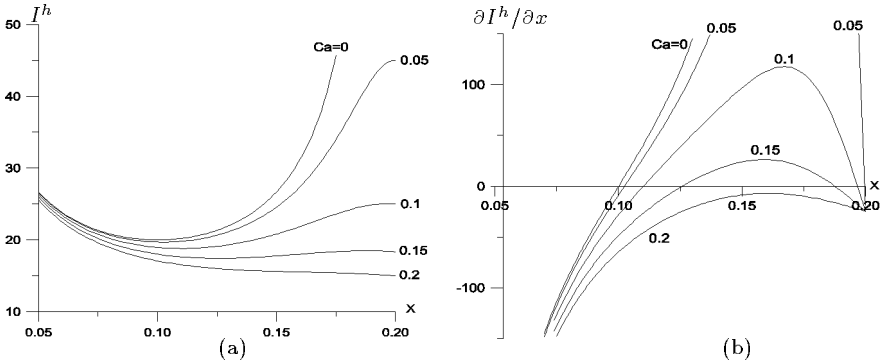

Fig.2. Dependence of the distribution for I^h (a) and $\partial I^h/\partial x$ (b) on c_a within the interval $(0, L)$. At c_a>0.185 minimization of I^h causes the right cell to collapse.

In order to preserve convexity of the functional we assume when varying x the derivative u_x in (2) remains fixed (invariable metric) as it was used in

[6]. Assuming in (6) the derivative $(u_x)_{i+1/2}$ not depending on x, we obtain the derivative of some new functional I_1^h

$$\frac{\partial I_1^h}{\partial x} = -\frac{1}{x^2} + \frac{1}{(L-x)^2\sqrt{1+c_a^2\triangle u^2/(L-x)^2}}\,. \tag{8}$$

To obtain an explicit expression of I_1^h, referred to as regularized functional, we integrate (8) and get

$$I_1^h = \frac{1}{x} + \frac{1}{c_a\triangle u} ln\left[\frac{c_a\triangle u}{L-x} + \sqrt{1+\frac{c_a^2\triangle u^2}{(L-x)^2}}\right]\,. \tag{9}$$

Distributions of I_1^h and $\partial I_1^h/\partial x$, presented in Fig.3, illustrate three important properties of this new class of functionals.

I. Functional I_1^h is convex within the interval (0,L) at any c_a.
II. At $c_a \to \infty$ position of x_{min} to I_1^h tends to L from the left.
III. There is an infinite barrier preventing the right cell from collapsing.

The first property guarantees existence of an unique solution of the variational problem within the interval $(0, L)$. The second property allows point 2 to approach point 3 at any small distance. The third one states that the infinite barrier keeps the mesh nondegenerate.

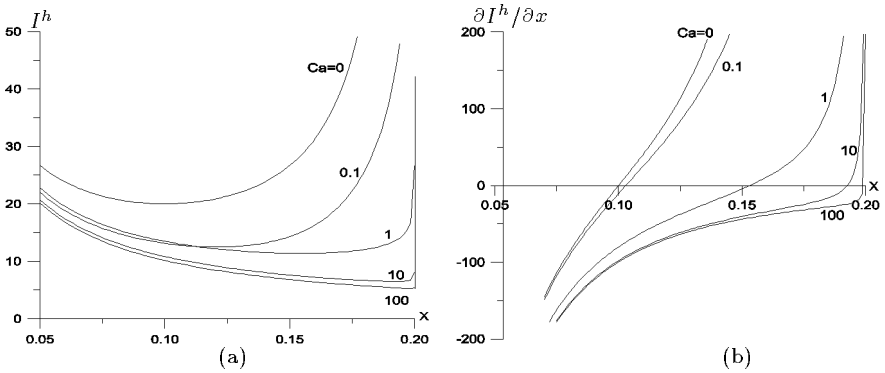

Fig.3. Dependence of the distribution for I_1^h (a) and $\partial I_1^h/\partial x$ (b) on c_a. Infinite barrier prevents the right cell from collapsing at any c_a.

Thus, the infinite barrier allows to condense the mesh in the vicinity of discontinuity up to any small distance. When modeling a flow with shock waves it provides the accuracy to increase significantly, since the error,

caused by shock wave smearing, in some integral norm is proportional to the shock thickness. Next corollary is that two adjacent cells, one located in the shock zone and the other in the domain of smooth flow, with sizes differing by orders of magnitude, do not deteriorate the accuracy of the solution. Thus, the mesh can sharply cluster, within one cell, towards a discontinuity. Those properties hold in case of any (even) number of intervals i_{max} as well.

Now we turn to a special case of constructing the 2-D adaptive mesh when the discrete functional can be reduced to one-parametric. Suppose the 2-D flow problem can be considered in 1-D approach. Then the control function in (1) depends only on the variable x. Therefore, when seeking the mapping of the parametric square to the domain Ω we have $x{=}x(\xi)$, $y{=}\eta$ and $f_y{=}x_\eta{=}y_\xi{=}0$. The harmonic functional (2) reads

$$(10) \qquad I = \int\int \frac{x_\xi^2(1+c_a^2 f_x^2)+1}{x_\xi\sqrt{1+c_a^2 f_x^2}} d\xi d\eta = \int \frac{x_\xi^2(1+c_a^2 f_x^2)+1}{x_\xi\sqrt{1+c_a^2 f_x^2}} d\xi \ .$$

The functional (10) differs from (2) by the additional term $\int x_\xi\sqrt{1+c_a^2 f_x^2}d\xi$ expressing the curve $c_a f$ length. This term defines the difference in properties of the 1-D and 2-D regularized discrete functionals.

We follow assumptions of Section 3. Approximation of (10) on the two-cell grid looks

$$I^h{=}\, x + \frac{1}{x} + (L-x)\sqrt{1+c_a^2\triangle u^2/(L-x)^2} + \frac{1}{(L-x)\sqrt{1+c_a^2\triangle u^2/(L-x)^2}} \ .$$

This functional holds the similar properties as (6). Within the interval $(0, L)$ at $c_a{<}c_a^{crt}$ there are maximum and minimum of I^h which disappear at $c_a{>}c_a^{crt}$. Here the value of c_a^{crt} differs a bit from above in 1-D case.

In order to regularize I^h we again fix the metric when deriving the first derivative. Derivative of a new functional reads

$$\frac{\partial I_1^h}{\partial x} \ = 1 - \frac{1}{x^2} - \sqrt{1+c_a^2\triangle u^2/(L-x)^2} + \frac{1}{(L-x)^2\sqrt{1+c_a^2\triangle u^2/(L-x)^2}} \ .$$

Integrating it we get the functional

$$I_1^h = \frac{1}{x} + x + \sqrt{(L-x)^2 + c_a^2\triangle u^2}$$

$$+\frac{1}{c_a\triangle u}(1-c_a^2\triangle u^2) ln\left[\frac{c_a\triangle u}{L-x} + \sqrt{1+\frac{c_a^2\triangle u^2}{(L-x)^2}}\right] \ .$$

Distributions of I_1^h and $\partial I_1^h/\partial x$ are presented in Fig.4. We see as soon as the expression $1-c_a^2\triangle u^2$ becomes negative, in the above case at $c_a>1/\triangle u=2$, the functional loses convexity. First, it seems to lead the right cell to collapse when finding the minimum of I_1^h via the iterative procedure (7). In practice it does not happen due to the following reason. If to derive the second derivative of I_1^h and substitute it and $\partial I_1^h/\partial x$ in (7), in the limit when point 2 tends to point 3, i.e. x tends to L, ratio of the derivatives gives $(L-x^p)(1-c_a^2\triangle u^2)/(1+c_a^2\triangle u^2)$. Thus, x^{p+1} gets the increment being smaller than distance to the right node $x_3=L$. Length of the right cell remains greater than zero within truncation error or prescribed accuracy of calculation at any $c_a>1/\triangle u$.

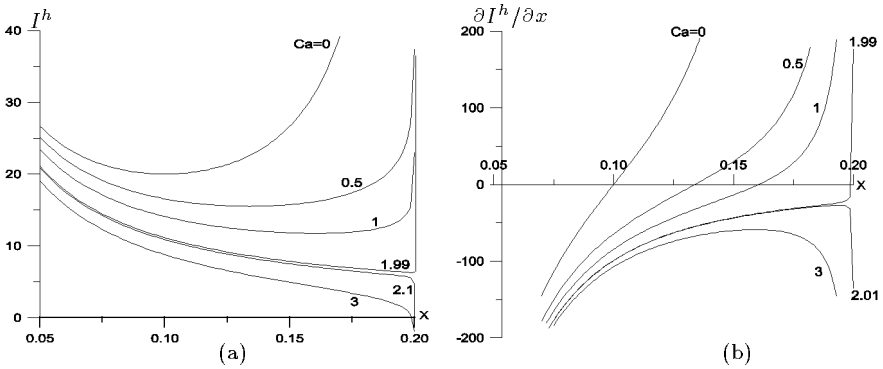

Fig.4. Quasi 1-D flow. Dependence of the distribution for I_1^h (a) and $\partial I_1^h/\partial x$ (b) on c_a. At $c_a>2$ the functional loses convexity.

Thus, it can turn out beginning from some value of c_a the regularized functional will not have the minimum. Nevertheless realization of the iterative procedure (7) allows to condense significantly the grid lines towards the discontinuity and guarantee the grid to be unfolded.

The above approach of three-point model of adaptation can be applied in general case when calculating real 2-D flows with discontinuities as well. Analysis based on this model is valid locally in every point of the discontinuity. When calculating the 2-D flows absence of the solution in multiparameter problem of minimization leads the grid nodes constantly to move along some trajectory around an average position keeping strong grid lines condensing in the vicinity of discontinuities. Further, for the sake of simplicity, we shall refer the procedure (7) (or its analogy in a real 2-D case) as a minimization of the discrete functional independently whether there is a solution of the minimization problem or not.

Performed analysis of the properties to the 1-D and 2-D functionals shows these functionals are inconsistent, i.e., grid clustering towards the discontinuity, executed inside the domain Ω via minimization of the 2-D functional and on the boundary $\partial\Omega$ via 1-D functional, is performed in different ways. It is arisen the necessity in consistent distribution of the grid nodes in Ω and on $\partial\Omega$.

5. Distribution of nodes along the boundary curve.

There are several ways to distribute the grid nodes along the boundary $\partial\Omega$ during adaptation. The simplest one, method I, is a fixed position of every point on $\partial\Omega$. When moving the internal nodes towards a discontinuity some instability in mesh generation arises, and consequently in the flow, near the points where the discontinuity joins $\partial\Omega$. In method II the boundary nodes are treated as internal and the vectors of shift are projected to $\partial\Omega$ [7]. This way can be used only if the discontinuity is orthogonal (or nearly orthogonal) to $\partial\Omega$. If no then, when condensing, the boundary nodes overlap, adjacent cells degenerate and modeling breaks. Method III consists in using the 1-D functional [5]. It is more robust than two above ways and usually can be used at adaptation. However, as it is shown in Section 4, the 1-D and 2-D discrete functionals are inconsistent. By this reason the parameters of adaptation c_a and τ should be selected to them separately. It requires additional work, which is particularly cumbersome when modeling unsteady flows. Sometimes we get undesirable displacement of the boundary nodes up to their overlap and then modeling stops.

It is required to perform distribution of the interior and boundary nodes consistently. In suggested method IV we perform constrained minimization of the functional (3) under constraints defining $\partial\Omega$. We minimize the following functional:

$$\tilde{I}^h = \sum_{i=1}^{i_{max}} \sum_{k=1}^{4} \frac{1}{4} [F_k]_i + \sum_{l \in \mathcal{L}} \lambda_l G_l = I^h + \sum_{l \in \mathcal{L}} \lambda_l G_l \ , \tag{11}$$

where constraints G_l=$G(x_l, y_l)$=0 define $\partial\Omega$, λ_l are the Lagrange multipliers, $\mathcal{L}$ is the set of the boundary nodes. Since the function $G(x, y)$ is assumed twice differentiable, the functional $\tilde{I}^h$ holds the infinite barrier on the boundary of the set of convex grids as I^h does (surely if $f \in C^1$).

If the set of convex grids is not empty, the system of algebraic equations has at least one solution being the mesh of convex quadrilaterals

$$R_x = \frac{\partial I^h}{\partial x_i} + \lambda_i \frac{\partial G_i}{\partial x_i} = 0 \ , \quad R_y = \frac{\partial I^h}{\partial y_i} + \lambda_i \frac{\partial G_i}{\partial y_i} = 0 \ , \quad G_i = 0 \ , \tag{12}$$

here i is a node number, λ_i=0 if $i \notin \mathcal{L}$ and constraints are defined only to the boundary nodes $i \in \mathcal{L}$.

Consider the method of minimizing the functional (11) assuming the grid to be convex at the p-th step of the iterative procedure. We use the quasi-Newton procedure to find the coordinates of the i-th node x_i^{p+1} and y_i^{p+1} from the system (12)

$$\tau R_x + \frac{\partial R_x}{\partial x_i}\,(x_i^{p+1} - x_i^p) + \frac{\partial R_x}{\partial y_i}\,(y_i^{p+1} - y_i^p) + \frac{\partial R_x}{\partial \lambda_i}\,(\lambda_i^{p+1} - \lambda_i^p) = 0 \ ,$$

$$(13)\quad \tau R_y + \frac{\partial R_y}{\partial x_i}\,(x_i^{p+1} - x_i^p) + \frac{\partial R_y}{\partial y_i}\,(y_i^{p+1} - y_i^p) + \frac{\partial R_y}{\partial \lambda_i}\,(\lambda_i^{p+1} - \lambda_i^p) = 0 \ ,$$

$$\tau G_i + \frac{\partial G_i}{\partial x_i}\,(x_i^{p+1} - x_i^p) + \frac{\partial G_i}{\partial y_i}\,(y_i^{p+1} - y_i^p) = 0 \ .$$

The procedure (13) can be also used when $\partial\Omega$ is given by parametric functions x=$x(t)$, y=$y(t)$ or tabular values $(x, y)_i$.

Another way, method V, of distributing the nodes along $\partial\Omega$, given by parametric functions, employs an unconstrained minimization and is based on solving the following system of algebraic equations:

$$R_t = R_x \frac{\partial x_i}{\partial t_i} + R_y \frac{\partial y_i}{\partial t_i} = 0 \ ,$$

via the quasi-Newton procedure

$$(14)\qquad \tau R_t + \frac{\partial R_t}{\partial t_i}\,(t_i^{p+1} - t_i^p) = 0 \ ,$$

here

$$\frac{\partial R_t}{\partial t_i} = \frac{\partial R_x}{\partial x_i}\left(\frac{\partial x_i}{\partial t_i}\right)^2 + \frac{\partial R_y}{\partial y_i}\left(\frac{\partial y_i}{\partial t_i}\right)^2 + \left(\frac{\partial R_x}{\partial y_i} + \frac{\partial R_y}{\partial x_i}\right)\frac{\partial x_i}{\partial t_i}\,\frac{\partial y_i}{\partial t_i}$$

$$+R_x \frac{\partial^2 x_i}{\partial t_i^2} + R_y \frac{\partial^2 y_i}{\partial t_i^2} \quad , \qquad R_x = \frac{\partial I^h}{\partial x_i} \quad , \qquad R_y = \frac{\partial I^h}{\partial y_i} \ .$$

Real-world 2-D flow computations have shown it is better to perform adaptation along the boundary using constrained minimization (13) since the procedure (14) does not always ensure consistent distribution of the nodes in Ω and on $\partial\Omega$.

6. Examples of modeling.

6.1 Analytic control function. First we shall demonstrate a simple test illustrating inconsistency of distributing the boundary and interior nodes performed using minimization of the 1-D and 2-D functionals, respectively.

The adapted mesh 50×50 has been generated in the unit square $0<x, y<1$ when the control function is defined as

$$f(x,y) = \begin{cases} 1 & \text{if} \quad y < 0.5 \ , \\ 0 & \text{if} \quad y \geq 0.5 \ . \end{cases}$$

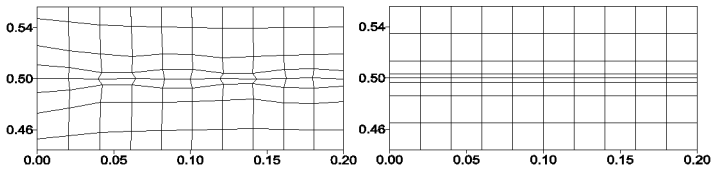

(a) (b)

Fig.5. Fragment of the adapted mesh when the boundary nodes are distributed using methods III (a) and IV (b).

Fragments of the adapted meshes in the vicinity of the discontinuity at c_a=0.1, obtained using methods III and IV, are presented in Fig.5a,b, respectively. In the first case the horizontal grid lines are not parallel and in the second they are parallel. In this test method II (and V) gives the same result as IV due to the discontinuity is orthogonal to $\partial\Omega$. But if it is not orthogonal in several tenths iterations the boundary nodes overlap.

6.2 Unsteady flow in a tunnel. Robustness of method IV is demonstrated in the test of the planar unsteady supersonic flow in the wind tunnel containing a step [12]. The wind tunnel is 1 unit wide and 3 units length, step is 0.2 units height and begins at x=0.6, see Fig.6. Initial conditions are $\boldsymbol{f}=(3,0,1,1.4)^T$, ratio of specific heats γ=1.4.

This test was calculated on the adapted grids when as a control function it was used various flow parameters [2]. The boundary nodes were adapted by using method III. One of the main difficulties was to capture the triple point, caused by irregular reflection of the bow shock from the top wall, with clustered grid lines that required especial user's effort.

In the present study the problem is calculated with the GLFC scheme of the second-order accuracy [1] on the adaptive moving mesh and $|V|$ is used as a control function. Figs. 6a,b present the mesh 180×60 and density contours at time t=4, respectively. Method IV of adaptation along the boundary allows to eliminate the above mentioned difficulty, see fragment IV of the mesh in Fig.6a, and to perform robust nodes clustering in the

domains where the shocks are attached to the boundary or reflect from it, see fragments $I - III$. We also obtained grid lines compression to the contact discontinuity, emanating from the triple point.

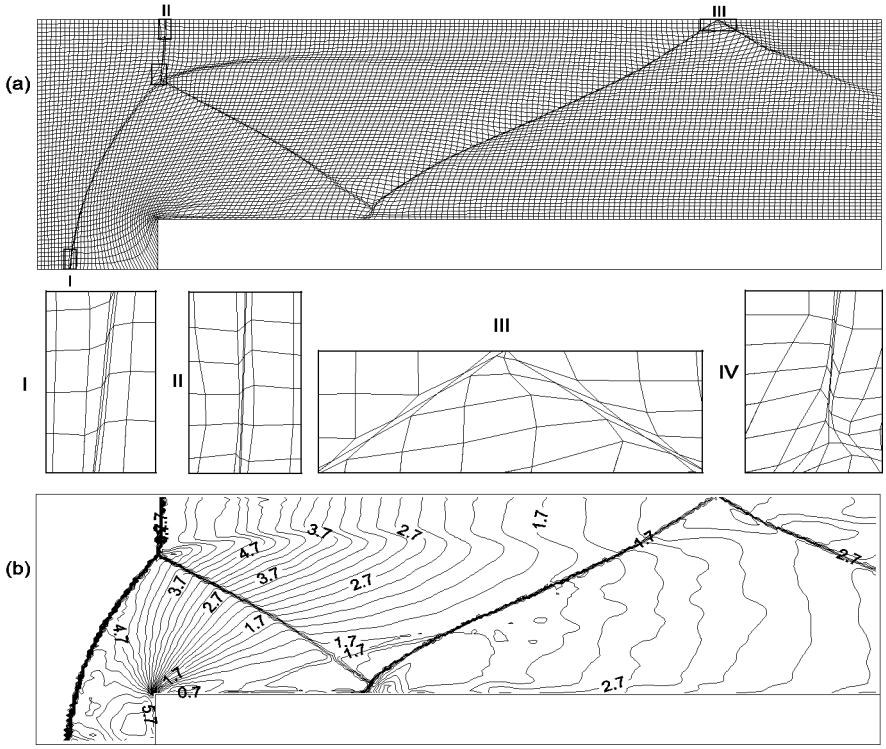

Fig.6. Supersonic flow in mach wind tunnel containing a step. Adapted mesh (a) with fragments I, II, III near the boundary and IV comprising the triple point. Density contours (b).

6.3 Flow over an airfoil. The GLFC scheme with adaptive procedure is applied to calculating steady transonic and supersonic Euler flow over the NACA0012 airfoil. Modeling is performed in two stages. At the first stage the calculation on the quasiuniform mesh, generated with the variational barrier method [5, 6], is performed until the solution achieves its steady state. Then, at the second stage, we switch on the adaptive procedure. As a control function it is used ρ.

The first test is a transonic case with M_∞=0.85 and angle of attack α=1°. Fig.7 presents the quasiuniform O-mesh 140×80 and plots the Mach number contours. We see that shock waves, one (stronger) on the upper

side of the airfoil and the other (weakear) on the low side, are rather thick. Fig.8 presents the adapted mesh and Mach number contours calculated on this grid. Adaptation of the boundary nodes is performed along the airfoil contour by applying method IV. Using method III or V leads the boundary nodes to overlap in the vicinity of shocks. Thickness of the shocks is reduced by 50 times in comparison with the nonadapted mesh that provides with capturing the discontinuities very accurately.

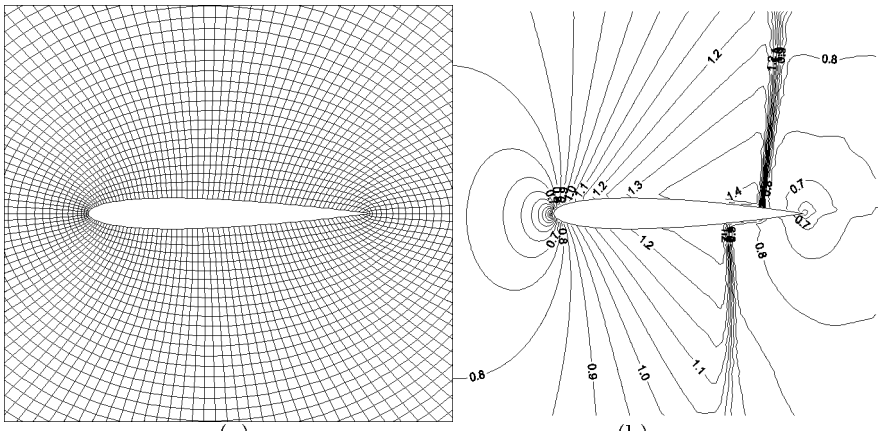

(a) (b)

Fig.7. Transonic flow around NACA0012 airfoil. Quasiuniform mesh (a) and Mach number contours (b).

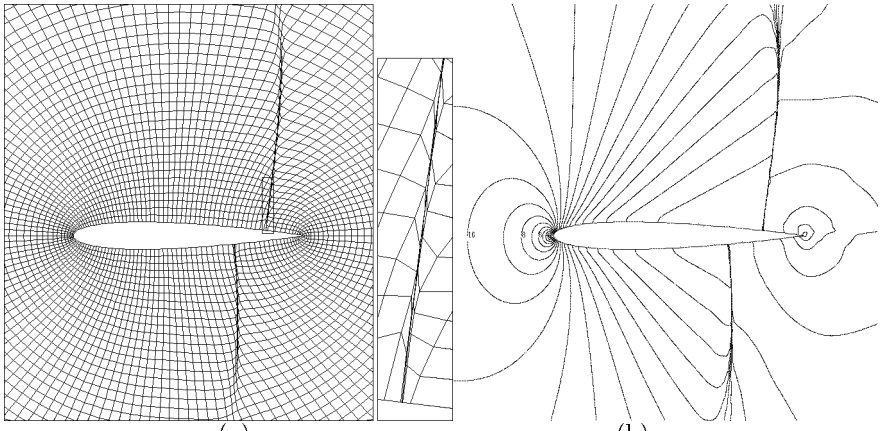

(a) (b)

Fig.8. Transonic flow around NACA0012 airfoil. Adapted mesh (a) and Mach number contours (b).

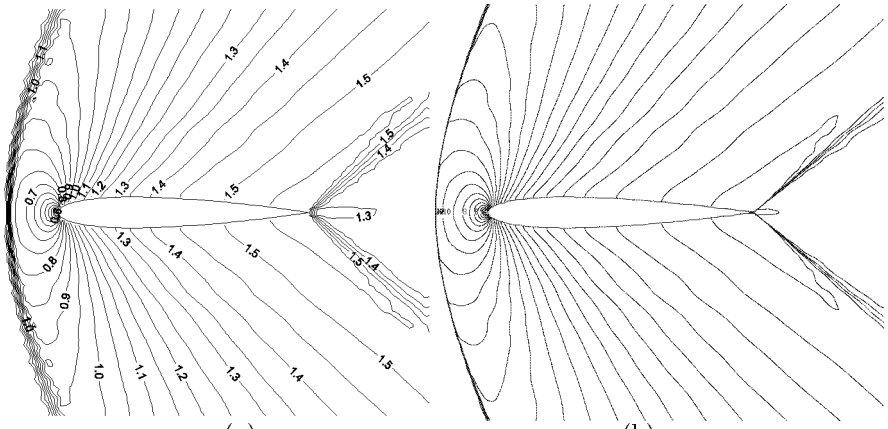

Fig.9. Supersonic flow around NACA0012 airfoil. Mach number contours computed on quasiuniform (a) and adapted (b) grids.

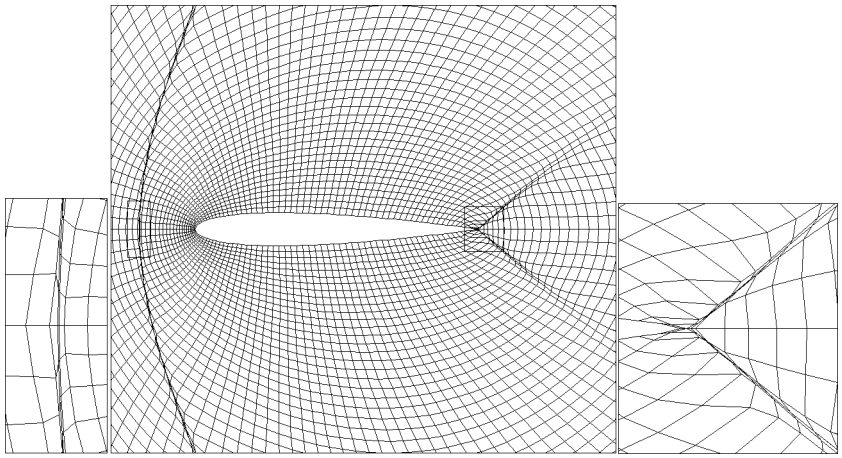

Fig.10. Mesh around NACA0012 airfoil after adaptation for supersonic flow calculations.

The other test is a supersonic flow with M_∞=1.3 and α=0°. Fig.9 plots the Mach number contours computed on the quasiuniform and adapted O-meshes 120×50. It can be seen in Fig.9a, a strong bow shock wave appears in front of the airfoil leading edge and two weak shocks emanate from the trailing edge. Using the adaptation provides with very strong reducing the thickness of the bow shock and rather strong reducing the thickness of the weaker trailing edge shocks that is demonstrated by the both Mach number

contours in Fig.9b and adapted grid in Fig.10. Grid lines clustering allows to hope that we nearly eliminate the errors caused by shock waves smearing and increase significantly the accuracy of computations.

7. Concluding remarks. Results of computations presented show adaptive-harmonic grid generation allows to increase significantly the accuracy of calculations in comparison with modeling on quasiuniform meshes due to reducing the thickness of smearing to the shock waves and contact discontinuities, while keeping the same simple grid structure and requiring less computing cost. Theoretical analysis based on the three-point model of adaptation has shown minimization of the regularized discrete functional in 1-D and 2-D cases delivers strong grid lines compression towards the discontinuities, while keeping the mesh unfolded. Constrained optimization leads to consistent distributing the boundary and interior mesh nodes that increases robustness of the adaptive procedure and modeling.

References

[1] B.N. Azarenok, Realization of a second-order Godunov's scheme, Comp. Meth. in Appl. Mech. and Engin. **189**, pp. 1031-1052 (2000).

[2] B.N. Azarenok and S.A. Ivanenko, Application of moving adaptive grids for numerical solution of nonstationary problems in gas dynamics, Int.J. for Numer. Meth. in Fluids, in press.

[3] J.U. Brackbill and J.S. Saltzman, Adaptive zoning for singular problems in two dimensions, J. Comp. Phys., **46**, 342-368 (1982).

[4] W.M. Cao, W.Z. Huang and R.D. Russel, A study of monitor functions for two dimensional adaptive mesh generation, SIAM J. Sci. Comput. **20**, pp. 1978-1994 (1999).

[5] A.A. Charakhch'yan and S.A. Ivanenko, A variational form of the Winslow grid generator, J. Comput. Phys. **136**, pp. 385-398 (1997).

[6] S.A. Ivanenko, Harmonic mappings, Chapt. 8 in Handbook of Grid Generation. J.F. Thompson et al (Eds.), CRC Press, Boca Raton, Fl., 1999.

[7] O-P. Jacquotte, Grid optimization methods for quality improvement and adaptation, Chapt. 33 in Handbook of Grid Generation.

[8] V.D. Liseikin, Grid Generation Methods, Springer-Verlag, New York, 1999.

[9] F. Liu, S. Ji, and G. Liao, An adaptive grid method and its application to steady Euler flow calculations, SIAM J. Sci. Comput. **20**, pp. 811-825 (1998).

[10] J.F. Thompson, A survey of dynamically-adaptive grids in the numerical solution of partial differential equations, Appl. Numer. Math., **1** pp. 3-27 (1985).

[11] A. Winslow, Numerical solution of the quasi-linear Poisson equation in a nonuniform triangle mesh, J. Comp. Phys. **1**, pp. 149-172 (1966).

[12] P. Colella and P.R. Woodward, The numerical simulation of two-dimensional fluid flow with strong shocks, J. Comput. Phys. **54**, pp. 115-173 (1984).